Changes in ocean denitrification during Late Carboniferous glacial–interglacial cycles

THOMAS ALGEO[1]*, HARRY ROWE[2], JAMES C. HOWER[2,3], LORENZ SCHWARK[4], ACHIM HERRMANN[5] AND PHIL HECKEL[6]

[1]Department of Geology, University of Cincinnati, Cincinnati, Ohio 45221-0013, USA
[2]Department of Earth and Environmental Sciences, University of Texas at Arlington, Arlington, Texas 76019, USA
[3]Center for Applied Energy Research, 2540 Research Park Drive, Lexington, Kentucky 40511, USA
[4]Institute for Geology and Mineralogy, University of Cologne, D-50674 Cologne, Germany
[5]Barrett Honors College, Arizona State University, Tempe, Arizona 85287, USA
[6]Department of Geoscience, University of Iowa, Iowa City, Iowa 52242, USA
*e-mail: thomas.algeo@uc.edu

Published online: 14 September 2008; doi:10.1038/ngeo307

Denitrification (the process by which nitrate and nitrite are reduced to nitrogen gas) in the oxygen-minimum zones of modern oceans is an important part of the global nitrogen cycle. Variations in rates of denitrification over Quaternary glacial–interglacial timescales may have affected global climate. Evidence of denitrification has been reported from some older marine systems, but it is unclear whether denitrification rates varied during pre-Quaternary glacial cycles. Here we present ratios of organic carbon to nitrogen and nitrogen isotope data from the Upper Carboniferous black shales of the North American mid-continent. In these cyclic deposits, we find evidence of variations in the intensity of denitrification in the eastern tropical Panthalassic Ocean associated with glacially driven sea-level changes. Sedimentary $\delta^{15}N$ increases during the interval of rapid sea-level rise in each cycle, indicative of intensified denitrification, before returning to background levels as sea level stabilized during the interglacial phase. Nearly identical patterns of denitrification have been observed in the eastern tropical Pacific during the Quaternary period. We therefore conclude that ice ages have produced similar oceanographic conditions and nitrogen cycle dynamics in these regions over the past 300 million years.

During the Permo-Carboniferous period, growth and decay of Gondwanan ice sheets caused large fluctuations (~50–150 m) in global sea level, or eustasy[1,2]. Such eustatic cycles yielded lithologically repetitive successions called cyclothems in the mid-continent region of North America[3,4]. Each 3- to 10-m-thick cyclothem contains a ~1-m-thick 'core' shale that is enriched in organic matter (to 40% total organic carbon (TOC)), trace metals and authigenic phosphate[5]. Core shales were deposited during glacio-eustatic highstands, when development of a strong, shallow pycnocline resulted in oxygen-deficient bottom waters in the Mid-continent Sea[3–6] (Fig. 1). Vertical stratification of the water column was favoured by a combination of palaeogeographic and palaeoclimatic factors: a nearly landlocked setting, limited tidality, and strong precipitation and runoff as a result of proximity to the palaeo-Intertropical Convergence Zone[5,6]. Circulation within the mostly <200-m-deep Mid-continent Sea exhibited a large-scale estuarine pattern, in which a westward-flowing, reduced-salinity surface layer (fed by runoff into the eastern end of the sea) overrode and entrained deep waters of normal-marine salinity. The sea was connected to the eastern tropical Panthalassic Ocean (ETPan) through a sinuous, ~1,000-km-long deep-water corridor in the greater Permian Basin region[6]. Intermediate waters of ETPan were drawn through this corridor and into the Anardarko Basin before welling up onto the western margin of the Mid-continent Shelf in present-day southern Kansas (Fig. 1).

We investigated three core shales of the North American Missourian Stage (Upper Pennsylvanian Series; ~303–305 Myr) of northeastern Kansas: the Hushpuckney, Stark and Muncie Creek (Fig. 2a). Sequence stratigraphic analysis shows that core shales comprise much of the transgressive, highstand and early regressive phases of mid-continent glacio-eustatic cycles[5]. In each cycle, the transgressive (deglacial) phase resulted in deposition of a thin basal limestone followed by black shale as increasing water depths caused anoxic waters below the pycnocline to advance in the direction of the shoreline[4,5]. The black shale facies is laminated and organic-rich (TOC >2.5%) and may be subdivided into a lower (LBS) and an upper subfacies (UBS) with a contact representing the maximum flooding surface (MFS) and corresponding to the deepest water (peak interglacial) conditions within each cycle (Fig. 2a). Above the MFS, the UBS exhibits a decrease in TOC and an increase in authigenic phosphate granules as a consequence of pycnoclinal weakening, increased vertical mixing and greater reworking of seafloor sediments during the early regressive phase (renewed glacial conditions)[5]. The UBS facies is overlain by a bioturbated, organic-poor (TOC <2.5%) grey shale facies that developed as continued sea-level fall caused anoxic waters below the pycnocline to shift

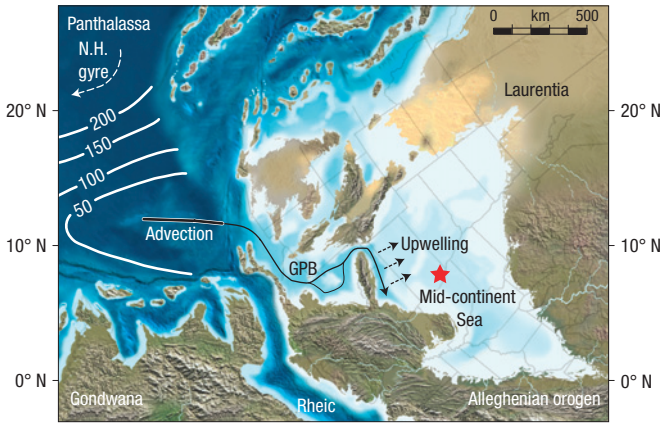

Figure 1 Palaeogeography of Late Carboniferous North America during interglacial sea-level highstands. The arrows show the pattern of lateral advection of denitrified suboxic waters from the eastern tropical Panthalassic Ocean through the greater Permian Basin (GPB) region and of upwelling onto the western margin of the Mid-continent Shelf. The red star indicates the location of the study units. The contours on the left show depth in metres of the 1 ml l^{-1} O_2 isocon (based on the modern ETPO (ref. 6)). The map is a Lambert azimuthal equal-area projection created by Ron Blakey. N.H. = Northen Hemisphere.

oceanward. Sedimentation rates were low, probably $\leq$8 mm kyr^{-1} (compacted), yielding duration estimates of $\sim$100($\pm$50) kyr for core shale accumulation[6]. Systematic variation in the thickness of centimetre-scale cycles within core shales implies nonlinear sediment accumulation rates, which decreased by a factor of two to three at the MFS relative to the base and top of core shales[5].

Patterns of chemostratigraphic variation within the three study units are similar. Several proxies, including TOC and trace-metal concentrations as well as degree-of-pyritization (DOP) and Fe_T/Al values, exhibit roughly symmetric first-order cycles through the black shale facies. These proxies exhibit low values at both the base and top of the black shale facies and reach maximum values at or near the MFS (Fig. 2b–d). Variation in these proxies was controlled primarily by depth-dependent changes in benthic (seafloor) redox conditions, with increases in water depth leading to intensified anoxia and higher proxy values. A secondary factor may have been pycnocline strength, which was controlled by humidity within the Mid-continent Sea watershed and the volume of freshwater runoff. Freshwater influx to the Mid-continent Sea can be estimated with F_{terr} (the terrigenous fraction of total organic matter; Fig. 2e; see Supplementary Information, Methods), which increased during more humid climatic intervals as larger quantities of organic matter were exported from coastal coal swamps[5]. F_{terr} generally peaks at or near the MFS, suggesting that humidity was greatest during interglacials and fell sharply in conjunction with climatic cooling at the onset of the following glacial stage.

C_{org}/N AND $\delta^{13}C$–$\delta^{15}N$ VARIATION IN CORE SHALES

C_{org}/N (the ratio of organic carbon to nitrogen) is commonly used as an indicator of organic matter provenance because marine algae exhibit lower values (4–10) than terrestrial higher plants (>20) (ref. 7). Total N covaries strongly with TOC (Fig. 2b), indicating that total N is a good proxy for organic N in organic-rich portions of the study units (Supplementary Information, Fig. S1). C_{org}/N ratios of 19–25 in the black shale facies (Fig. 2f) might be interpreted as evidence of the predominance of terrigenous organic matter, but Rock-Eval data indicate the presence of subequal amounts of marine and terrigenous organic matter (Supplementary Information, Fig. S2). C_{org}/N is significantly correlated with F_{terr} ($r = +0.26$; $p(\alpha) < 0.01$; $n = 103$), yielding estimated C_{org}/N ratios of $\sim$19–23 and $\sim$21–25 for the marine and terrigenous endmembers, respectively (Supplementary Information, Figs S3,S4). The high C_{org}/N ratios of the marine organic fraction are due to some combination of preferential bacterial destruction of labile N-bearing compounds[8] and production of algal biomass with a C/N ratio in excess of the Redfield ratio (6–7), as in some modern ocean-surface waters in which productivity is limited by bioavailable N (refs 9,10). C_{org}/N ratios in the grey shale facies are mostly 6–12 (Fig. 2f), values that may reflect a large fraction of mineral N in organic-poor samples.

In contrast to the proxies discussed above, the C- and N-isotope records of the study units exhibit strongly asymmetric first-order cycles, in which excursion peaks are located just above the base of the LBS. Each $\delta^{13}C_{org}$ record exhibits an about $-$3‰ excursion to a minimum of $-$28 to $-$29‰ (Fig. 2g), whereas each $\delta^{15}N_{tot}$ record exhibits a +5 to +9‰ excursion to a maximum of +10 to +14‰ (Fig. 2h). Above the excursion peaks, there is a gradual return to background values of $-$25 to $-$26‰ for $\delta^{13}C_{org}$ and +4 to +6‰ for $\delta^{15}N_{tot}$. Within each study unit, $\delta^{13}C_{org}$ and $\delta^{15}N_{tot}$ covary negatively within the LBS facies but exhibit no relationship within the UBS and grey shale facies (Fig. 3). One feature of both the C- and N-isotope records is limited sample-to-sample variance, which is in sharp contrast to the pronounced intersample variance observed in the TOC, DOP, Fe_T/Al and F_{terr} records (Fig. 2b–e). As a result, $\delta^{13}C_{org}$ and $\delta^{15}N_{tot}$ exhibit a smooth clockwise pattern of covariation in two of the three study units (Hushpuckney, Muncie Creek), revealing that changes in $\delta^{15}N_{tot}$ preceded changes in $\delta^{13}C_{org}$ during both the intensification and relaxation phases of each isotopic excursion (Fig. 3).

Sedimentary organic N commonly reflects the isotopic signature of fixed N in the water mass of origin[11–21]. Fixed N in the modern ocean has a residence time of $\sim$1.5 kyr (refs 22,23), similar to timescales of oceanic mixing, and, hence, exhibits moderate isotopic variation. The $\delta^{15}N$ composition of nitrate (NO_3^-) in the deep ocean is fairly uniform (+4 to +6‰) (refs 23,24), but surface- to intermediate-depth waters exhibit $\sim$20‰ variation owing to the localized effects of fractionation during assimilatory uptake, N fixation and denitrification[17,18,25,26]. Assimilatory uptake raises the $\delta^{15}N$ composition of seawater nitrate owing to a about $-$5‰ fractionation associated with this process[25], but the effect is pronounced only in areas of low to moderate productivity and generally does not exceed a few per mille[26]. N fixation, in which gaseous N_2 with a $\delta^{15}N$ of $\sim$0‰ is converted to a bioavailable form with little or no fractionation[23], can lower the $\delta^{15}N$ of seawater nitrate[20]. Conversely, denitrification, in which bacteria selectively use ^{15}N-depleted nitrate as an oxidant with a fractionation of $-$22 to $-$30‰, can produce a water mass with substantially ^{15}N-enriched residual nitrate[20,23]. The latter process is important in oxygen-minimum zones (OMZs) associated with continent-margin upwelling zones, as in the Arabian Sea and eastern tropical Pacific Ocean (ETPO), with the latter accounting for about 2/3 of all water-column denitrification and resulting in seawater nitrate $\delta^{15}N$ values locally >15‰ (refs 22,23). The anammox reaction, in which nitrite (NO_2^-) reacts with ammonium, contributes to overall rates of denitrification in sea water but is thought to have little influence on the isotopic composition of bioavailable nitrogen[27].

PALAEOCEANOGRAPHIC CIRCULATION

Denitrified water masses can be advected over considerable distances and still retain their characteristic isotopic signatures,

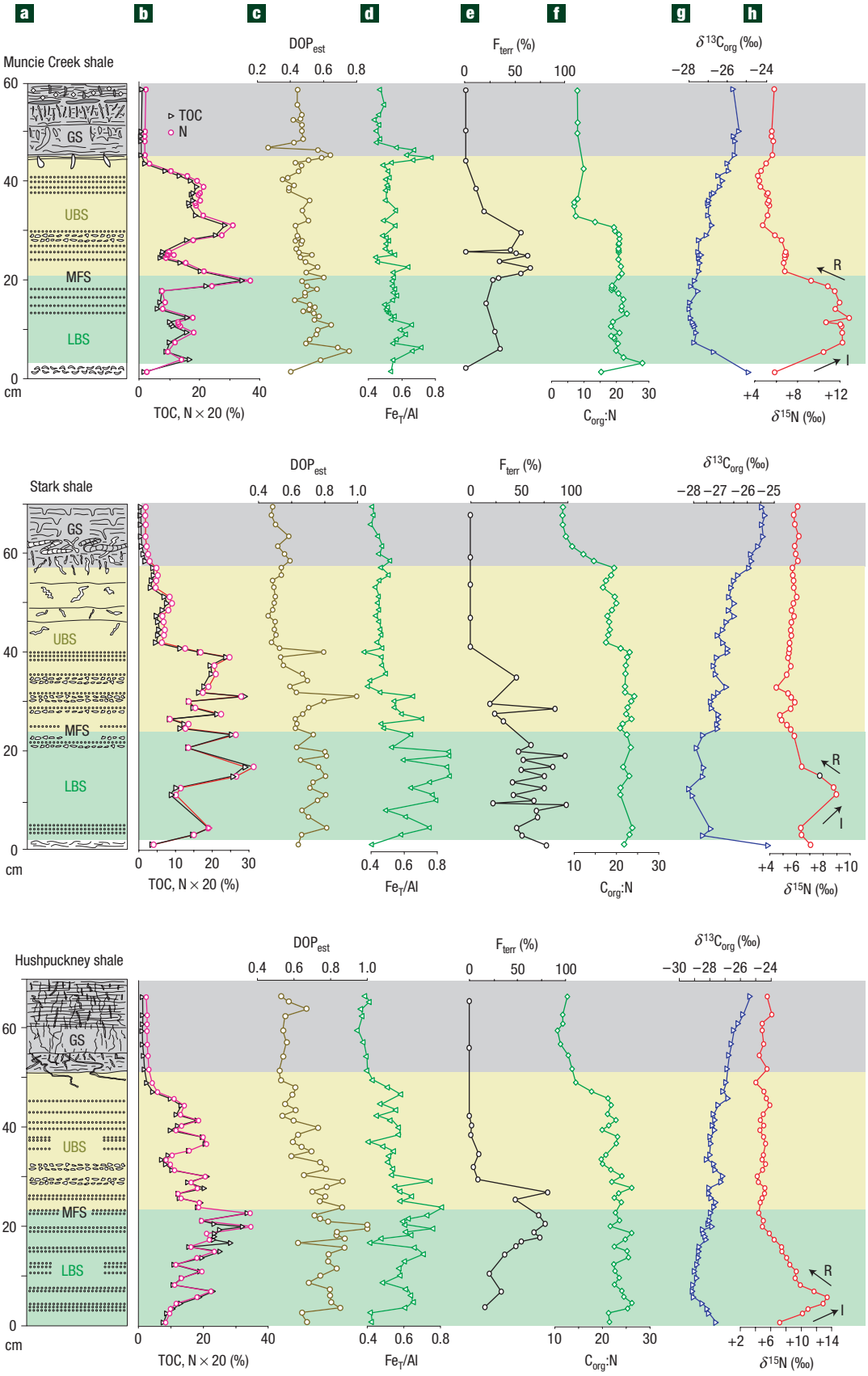

Figure 2 Study sections. **a**, Sedimentary features. **b**, TOC and N. **c**, DOP_{est}. **d**, Fe_T/Al. **e**, F_{terr}. **f**, C_{org}/N (molar ratio). **g**, $\delta^{13}C_{org}$. **h**, $\delta^{15}N_{tot}$. I and R show the intensification and relaxation phases of the isotopic excursions, respectively. LBS = lower black shale, UBS = upper black shale, GS = grey shale and MFS = maximum flooding surface.

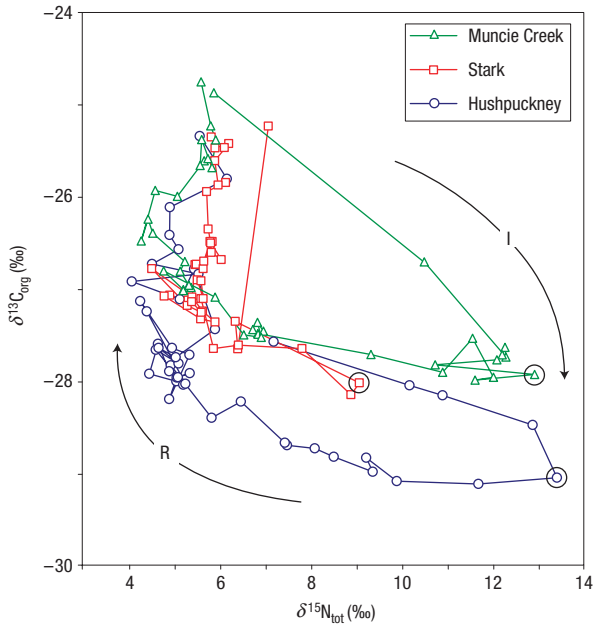

Figure 3 $\delta^{15}N_{tot}$ versus $\delta^{13}C_{org}$ for study units. Arrows indicate upsection sequence of samples; I and R as in Fig. 2. Circled samples represent excursion peaks, corresponding to maximum rates of advection of denitrified water masses into the Late Pennsylvanian Mid-continent Sea.

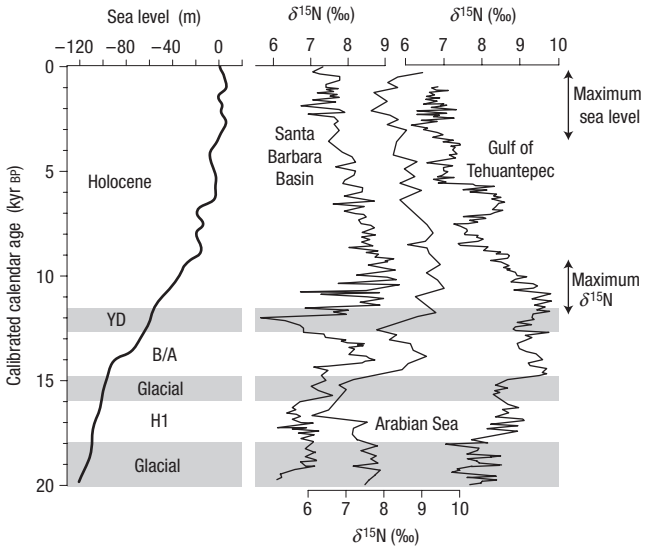

Figure 4 Sea-level curve and upwelling-zone $\delta^{15}N$ data for 20 kyr BP to present. Shading indicates colder intervals; YD = Younger Dryas, B/A = Bölling–Allerød, H1 = Heinrich-1 event. Sources: Sea-level curve[30], Santa Barbara Basin[45], Arabian Sea[14], Gulf of Tehuantepec[19].

which thus can be transferred to the sediment far from any site of active denitrification. Along the western margin of North America, Quaternary sediments as far north as Oregon exhibit ^{15}N enrichment linked to northward advection by the California Undercurrent of denitrified waters from the ETPO, >1,000 km to the south[15,18,28]. Transport of denitrified water masses over comparable distances has been reported from other modern marine systems as well[29]. On the basis of these examples of long-range advection within the global ocean, the transfer of denitrified water masses from the ETPan to the Mid-continent Sea through a confined, ~1,000-km-long marine corridor (the greater Permian Basin seaway) seems entirely feasible (Fig. 1). Owing to their strongly oxygen-deficient character, advection and upwelling of such denitrified water masses onto the Mid-continent Shelf may have been a key factor in the development of intensely anoxic and sulphidic conditions during deposition of Upper Carboniferous cyclothemic core shales[5,6].

Studies of sediment cores from modern marine upwelling systems in the Arabian Sea[11–14] and ETPO (refs 15–19,28) have revealed pronounced glacial–interglacial variations in organic-N isotopes. In these settings, $\delta^{15}N_{org}$ values were +6 to +8‰ during the Last Glacial Maximum (~18 kyr BP) but rose as much as 12‰ by ~14 kyr BP (Fig. 4). Subsequently, $\delta^{15}N_{org}$ values declined gradually, and modern surface sediments yield values close to those seen during the Last Glacial Maximum. The excursion peak in these records comes mid way through the deglacial rise in global sea level, and the return to values typical of average sea water was effectively completed during the present interglacial highstand (Holocene). This pattern of glacial–interglacial variation in $\delta^{15}N_{org}$ has been shown to recur through multiple Quaternary glacial cycles and, thus, represents an integral component of marine feedbacks to orbital forcing[15,28]. The relationship of climate and sea-level elevation[30] to sediment N-isotopic variation in these modern systems is almost identical to that in the three study units, in each of which $\delta^{15}N_{tot}$ rose sharply to +10 to +14‰ in conjunction with the deglacial transgression, before returning gradually to background values of +4 to +6‰ (Fig. 2h). The relaxation phase of each isotopic excursion was completed before the sea-level highstand (MFS) associated with fully interglacial conditions (Fig. 2a).

The C_{org}- and N-isotopic records of the study units differ from those of modern marine upwelling systems in one significant detail: the latter exhibit substantial high-frequency millennial-scale variations[14,19,20] whereas the former do not (Fig. 2g,h) despite pronounced centimetre-scale variation in other geochemical proxies (Fig. 2b–e). Such high-frequency variation is a signature of short-term climatic influences on a local marine environment, and its absence in the C_{org}- and N-isotopic records of the study units, in combination with strong $\delta^{13}C_{org}$–$\delta^{15}N_{tot}$ covariation (Fig. 3), implies control not by local processes within the Mid-continent Sea but rather by a long-range process that suppressed high-frequency environmental variation. A mechanism that is consistent with palaeogeographic reconstructions[6] is isolation and mixing of denitrified ETPan intermediate waters during long-distance (>1,000 km) transport through the greater Permian Basin seaway before upwelling beneath the pycnocline of the Mid-continent Sea (Fig. 1).

PALAEOCLIMATE CONTROLS AND SIGNIFICANCE

Several hypotheses have been advanced concerning glacial–interglacial variation in the denitrification rates of Quaternary marine upwelling systems. One possibility is that continental warming resulted in an intensified land–sea thermal contrast and stronger offshore winds during the early stages of deglaciation, enhancing upwelling of nutrient-rich intermediate ocean waters and causing productivity-driven expansion of the OMZ (refs 15,16). Alternatively, changes in ocean circulation may have influenced denitrification rates through changes in the ventilation or flux of laterally advected intermediate water masses[28,31–33]. For example, decreased advection of South Pacific Intermediate Water beneath the Equatorial Undercurrent during

the last deglaciation may have reduced ventilation of ETPO intermediate waters, an inference supported by variance in sediment N-isotopic records at a 41 kyr frequency (a high-latitude signal)[28,31,32]. Variation in the flux of Pacific Intermediate Water to the ETPO at depths below 600 m may also have been important[15,33]. In view of the similarity in geographic boundary conditions (Fig. 1), mechanisms based on variable rates of either wind-driven upwelling or intermediate-water ventilation can potentially account for fluctuations in denitrification rates in the Late Carboniferous ETPan.

The causes of declining sediment $\delta^{15}N_{org}$ values during the late stages of Quaternary deglacial transgressions (Fig. 4) are uncertain. One hypothesis is that denitrification led to N-poor conditions that favoured cyanobacterial N fixers[34], the isotopically light N input of which ($\delta^{15}N = -1$ to $+1$‰) then diluted the isotopic signal of denitrification[19]. However, this hypothesis does not account for patterns of negative covariation between $\delta^{13}C_{org}$ and $\delta^{15}N$ in modern upwelling systems[15] or in the study units (Fig. 3). Such covariation suggests an alternative hypothesis linking upwelling intensity to changes in primary productivity in the ETPO/ETPan. The observation that changes in $\delta^{15}N_{tot}$ lead those in $\delta^{13}C_{org}$ during both the intensification and relaxation phases of each N-isotopic excursion (Fig. 3) may indicate that changes in productivity responded to changes in upwelling intensity throughout each glacial cycle, and that the main cause of declining $\delta^{15}N_{tot}$ values during the later stages of deglacial transgressions was weaker upwelling.

Other interpretations of the N-isotope records of the study units are less likely. Both the intensification and relaxation phases of each isotopic excursion occurred under transgressive conditions (Fig. 2a), indicating that eustatic forcing of OMZ depth was not the primary control on $\delta^{15}N_{tot}$ variation. Changes in freshwater influx into the Mid-continent Sea and attendant dilutional effects are unlikely to have been an important factor, because there is little relationship between F_{terr} (a proxy for freshwater influx) and $\delta^{15}N_{tot}$ (Fig. 2e,h). Fractionation during assimilatory uptake can lead to higher $\delta^{15}N_{org}$ values through Rayleigh distillation where biotic utilization of [NO_3^-] is incomplete[25,26]. However, this process is characteristic of intra-oceanic high-nutrient low-chlorophyll regions rather than continent-margin upwelling zones, where virtually all bioavailable N is used on an interannual basis[14,17]. Fractionation during denitrification in the sediment can lead to higher $\delta^{15}N_{NO3-}$ values, but the upward diffusive flux of pore-water nitrate is insufficient to alter the isotopic composition of nitrate in the overlying water column[35]. A lack of TOC–$\delta^{15}N_{tot}$ covariation in the study units (Fig. 2b,h) suggests that N-isotopic values were not strongly influenced by primary productivity within the Mid-continent Sea itself, although relationships to productivity in the ETPan cannot be determined. Finally, destruction of organic matter within the water column or during early diagenesis can alter $\delta^{15}N_{org}$ values in the sediment, but this effect is generally no more than ±4‰ in oxic environments[8,21,36] and tends to be less in high-productivity settings in which organic matter is better preserved[13–15,20]. The UBS and grey shale facies of the study units yield identical $\delta^{15}N_{tot}$ values ($+4$ to $+6$‰; Fig. 2h), which demonstrates the absence of a differential isotopic shift as a function of benthic redox conditions.

Comparison of the N-isotope records of the study units with those of modern continent-margin upwelling systems has important implications for an understanding of the global N cycle during ice ages. First, changes in OMZ denitrification rates associated with glacial–interglacial cycles may act as a positive feedback mechanism for global climate change[12–15,17,19]. At the onset of deglaciation, intensified denitrification within OMZs reduces the global seawater nitrate inventory, thus decreasing the biological pump that transfers carbon to the deep ocean, leading to higher atmospheric CO_2 concentrations and further climatic warming[15]. A secondary effect of intensified denitrification is increased production of N_2O (ref. 37), a greenhouse gas that is 300 times more potent than CO_2 (ref. 38) and that exhibits pronounced variation in conjunction with glacial–interglacial cycles[39]. The similarity of the N-isotope records of the study units to those of modern marine upwelling systems suggests that a similar positive feedback operated during Carboniferous glacial–interglacial cycles.

Second, the background $\delta^{15}N_{tot}$ values of the study units ($+4$ to $+6$‰, in the UBS and grey shale facies) are similar to those of modern seawater nitrate and sediment $\delta^{15}N_{org}$ values in non-upwelling areas[23–26] but markedly different from the background values in Jurassic and Cretaceous black shales, which are mostly between -2 and $+2$‰ (refs 40–43). Explanations for this pattern of secular variation include: (1) changes in the relative global importance of water-column versus pore-water denitrification, with the latter yielding lower seawater nitrate $\delta^{15}N$ values owing to reduced fractionation (-3 to 0‰) as a consequence of diffusion-limited nitrate supply in sediments[23,44], and (2) changes in global N fixation rates, with enhanced N fixation yielding lower seawater nitrate $\delta^{15}N$ values. Higher background $\delta^{15}N$ values, as in the Quaternary and Carboniferous, are consistent with higher globally integrated rates of water-column denitrification and/or lower rates of N fixation. The results of the present study are significant in providing evidence that global N budgets were similar during ice ages over the past 300 million years and different from global N budgets during warm-climate periods such as the Jurassic and Cretaceous.

METHODS

The study units were sampled in the Kansas Geological Survey, Orville Edmonds No. 1A drillcore, from Leavenworth County, Kansas (Sec. 35, Twp. 9S, Range 22E)[5]. A total of 51, 50 and 70 samples were collected from the Hushpuckney, Stark and Muncie Creek shales, respectively, at an average spacing of ~1 cm in the black shale facies and ~2.5 cm in the grey shale facies of each unit. Trace-element concentrations were determined at the University of Cincinnati using a wavelength-dispersive Rigaku 3040 X-ray fluorescence spectrometer and calibrated using both United States Geological Survey and internal black shale standards; analytical precision (2σ) was better than ±5% of reported values. C and N elemental and stable isotopic compositions were determined at the University of Kentucky Environmental Research Training Laboratory using a Costech 5010 elemental analyser coupled through a Conflo-III device to a ThermoFinnigan Delta*Plus* XP isotope-ratio-mass spectrometer. Analytical precision was 0.08% for %N, 0.07% for %C, 0.05‰ for $\delta^{15}N$ and 0.09‰ for $\delta^{13}C$ of standards. All isotopic results are reported relative to air ($\delta^{15}N$) and Vienna PeeDee Belemnite ($\delta^{13}C$). See Supplementary Information, Methods for details of organic petrography and Fe–S system analyses.

Received 28 May 2008; accepted 13 August 2008; published 14 September 2008.

References

1. Soreghan, G. S. & Giles, K. A. Amplitudes of Late Pennsylvanian glacioeustasy. *Geology* **27**, 255–258 (1999).
2. Joachimski, M. M., von Bitter, P. H. & Buggisch, W. Constraints on Pennsylvanian glacio-eustatic sea-level changes using oxygen isotopes of conodont apatite. *Geology* **34**, 277–280 (2006).
3. Heckel, P. H. Sea-level curve for Pennsylvanian eustatic marine transgressive-regressive depositional cycles along midcontinent outcrop belt, North America. *Geology* **14**, 330–334 (1986).
4. Heckel, P. H. in *Modern and Ancient Continental Shelf Anoxia* (eds Tyson, R. V. & Pearson, T. H.) 259–273 (Spec. Publ. 58, Geol. Soc. London, Oxford, 1991).
5. Algeo, T. J., Schwark, L. & Hower, J. C. High-resolution geochemistry and sequence stratigraphy of the Hushpuckney Shale (Swope Formation, eastern Kansas): Implications for climato-environmental dynamics of the Late Pennsylvanian Midcontinent Sea. *Chem. Geol.* **206**, 259–288 (2004).
6. Algeo, T. J., Heckel, P. H., Maynard, J. B., Blakey, R. & Rowe, H. in *Dynamics of Epeiric Seas: Sedimentological, Paleontological and Geochemical Perspectives* (eds Holmden, C & Pratt, B R) (Spec. Publ., Geol. Assoc., Canada, 2007) in the press.
7. Meyers, P. A. Preservation of elemental and isotopic source identification of sedimentary organic matter. *Chem. Geol.* **114**, 289–302 (1994).
8. Prokopenko, M. G. *et al.* Nitrogen cycling in the sediments of Santa Barbara basin and Eastern Subtropical North Pacific: Nitrogen isotopes, diagenesis and possible chemosymbiosis between two lithotrophs (*Thioploca* and Anammox)—riding on a glider. *Earth Planet. Sci. Lett.* **242**, 186–204 (2006).
9. Hansell, D. A. & Waterhouse, T. Y. Controls on the distributions of organic carbon and nitrogen in the eastern Pacific Ocean. *Deep-Sea Res. I* **44**, 843–857 (1997).

10. Copin-Montégut, C. Consumption and production on scales of a few days of inorganic carbon, nitrate and oxygen by the planktonic community: Results of continuous measurements at the Dyfamed Station in the northwestern Mediterranean Sea (May 1995). *Deep-Sea Res. I* **47**, 447–477 (2000).
11. François, R., Altabet, M. A. & Burckle, L. H. Glacial to interglacial changes in surface nitrate utilization in the Indian section of the Southern Ocean as recorded by sediment δ^{15}N. *Paleoceanography* **7**, 589–606 (1992).
12. Altabet, M. A., François, R., Murray, D. W. & Prell, W. L. Climate-related variations in denitrification in the Arabian Sea from sediment ^{15}N/^{14}N ratios. *Nature* **373**, 506–509 (1995).
13. Altabet, M. A., Higginson, M. J. & Murray, D. W. The effect of millennial-scale changes in Arabian Sea denitrification on atmospheric CO_2. *Nature* **415**, 159–162 (2002).
14. Suthhof, A., Ittekkot, V. & Gaye-Haake, B. Millennial-scale oscillation of denitrification intensity in the Arabian Sea during the late Quaternary and its potential influence on atmospheric N_2O and global climate. *Glob. Biogeochem. Cycles* **15**, 637–649 (2001).
15. Ganeshram, R. S., Pedersen, T. F., Calvert, S. E., McNeill, G. W. & Fontugne, M. R. Glacial-interglacial variability in denitrification in the world's oceans: Causes and consequences. *Paleoceanography* **15**, 361–376 (2000).
16. Ganeshram, R., Pedersen, T., Calvert, S. & François, R. Reduced nitrogen fixation in the glacial ocean inferred from changes in marine nitrogen and phosphorus inventories. *Nature* **415**, 156–159 (2002).
17. Pride, C. *et al*. Nitrogen isotopic variations in the Gulf of California since the last deglaciation: Response to global climate change. *Paleoceanography* **14**, 397–409 (1999).
18. Kienast, S. S., Calvert, S. E. & Pedersen, T. Nitrogen isotope and productivity variations along the northeast Pacific margin over the last 120 kyr: Surface and subsurface paleoceanography. *Paleoceanography* **17**, 1–17 (2002).
19. Thunell, R. C. & Kepple, A. B. Glacial-Holocene δ^{15}N record from the Gulf of Tehuantepec, Mexico: Implications for denitrification in the eastern equatorial Pacific and changes in atmospheric N_2O. *Glob. Biogeochem. Cycles* **18**, GB1001 (2004).
20. Voss, M., Dippner, J. W. & Montoya, J. P. Nitrogen isotope patterns in the oxygen-deficient waters of the Eastern Tropical Pacific Ocean. *Deep-Sea Res. I* **48**, 1905–1921 (2001).
21. Altabet, M. A. & François, R. Sedimentary nitrogen isotopic ratio as a recorder for surface ocean nitrate utilization. *Glob. Biogeochem. Cycles* **8**, 103–116 (1994).
22. Gruber, N. & Sarmiento, J. L. Global patterns of marine nitrogen fixation and denitrification. *Glob. Biogeochem. Cycles* **11**, 235–266 (1997).
23. Brandes, J. A. & Devol, A. H. A global marine-fixed nitrogen isotopic budget: Implications for Holocene nitrogen cycling. *Glob. Biogeochem. Cycles* **16**, 1120 (2002).
24. Sigman, D. M., Altabet, M. A., François, R., McCorkle, D. C. & Gaillard, J.-F. The isotopic composition of diatom-bound nitrogen in Southern Ocean sediments. *Paleoceanography* **14**, 118–134 (1999).
25. Sigman, D. M., Altabet, M. A., McCorkle, D. C., François, R. & Fischer, G. The δ^{15}N of nitrate in the Southern Ocean: Consumption of nitrate in surface waters. *Glob. Biogeochem. Cycles* **13**, 1149–1166 (1999).
26. Holmes, M. E., Fischer, G., Lavik, G. & Wefer, G. in *South Atlantic in the Late Quaternary; Reconstruction of Material Budgets and Current Systems* (eds Mulitza, S. & Ratmeyer, V.) 143–165 (Springer, Berlin, 2003).
27. Murray, J. W., Fuchsman, C., Kirkpatrick, J., Paul, B. & Konovalov, S. K. Species and δ^{15}N signatures of nitrogen transformations in the suboxic zone of the Black Sea. *Oceanography* **18**, 36–47 (2005).
28. Liu, Z., Altabet, M. A. & Herbert, T. D. Glacial–interglacial modulation of eastern tropical North Pacific denitrification over the last 1.8-Myr. *Geophys. Res. Lett.* **32**, L23607 (2005).
29. Higginson, M. J., Maxwell, J. R. & Altabet, M. A. Nitrogen isotope and chlorin paleoproductivity records from the Northern South China Sea: Remote versus local forcing of millennial- and orbital-scale variability. *Mar. Geol.* **201**, 223–250 (2003).
30. Siddall, M. *et al*. Sea-level fluctuations during the last glacial cycle. *Nature* **423**, 853–858 (2003).
31. Andreasen, D. H., Ravelo, A. C. & Broccoli, A. J. Remote forcing at the Last Glacial Maximum in the tropical Pacific Ocean. *J. Geophy. Res.* **106**, 879–897 (2001).
32. Meissner, K. J., Galbraith, E. D. & Volker, C. Denitrification under glacial and interglacial conditions: A physical approach. *Paleoceanography* **20**, PA3001 (2005).
33. Zheng, Y., van Geen, A., Anderson, R., Gardner, J. & Dean, W. Intensification of the northeast Pacific oxygen minimum zone during the Bölling/Allerød warm period. *Paleoceanography* **15**, 528–536 (2000).
34. Karl, D. *et al*. The role of nitrogen fixation in biogeochemical cycling in the subtropical North Pacific Ocean. *Nature* **388**, 533–538 (1997).
35. Sigman, D. M. *et al*. Distinguishing between water column and sedimentary denitrification in the Santa Barbara Basin using the stable isotopes of nitrate. *Geochem. Geophys. Geosyst.* **4**, 1040 (2003).
36. Lehmann, M. F., Bernasconi, S. M., Barbieri, A. & McKenzie, J. A. Preservation of organic matter and alteration of its carbon and nitrogen isotope composition during simulated and *in situ* early sedimentary diagenesis. *Geochim. Cosmochim. Acta* **66**, 3573–3584 (2002).
37. Naqvi, S. W. A. *et al*. Budgetary and biogeochemical implications of N_2O isotope signatures in the Arabian Sea. *Nature* **394**, 462–464 (1998).
38. Lashof, D. A. & Ahuja, R. D. Relative contributions of greenhouse gas emissions to global warming. *Nature* **344**, 529–531 (1990).
39. Flückiger, J. *et al*. Variations in atmospheric N_2O concentration during abrupt climatic changes. *Science* **285**, 227–230 (1999).
40. Jenkyns, H. C., Gröcke, D. R. & Hesselbo, S. P. Nitrogen isotope evidence for water mass denitrification during the early Toarcian (Jurassic) oceanic anoxic event. *Paleoceanography* **16**, 593–603 (2001).
41. Rau, G. H., Arthur, M. A. & Dean, W. E. ^{15}N/^{14}N variations in Cretaceous Atlantic sedimentary sequences: Implication for past changes in marine nitrogen biogeochemistry. *Earth Planet. Sci. Lett.* **82**, 269–279 (1987).
42. Saelen, G., Tyson, R. V., Telnaes, N. & Talbot, M. R. Contrasting watermass conditions during deposition of the Whitby Mudstone (Lower Jurassic) and Kimmeridge Clay (Upper Jurassic) formations, UK. *Palaeogeogr. Palaeoclimatol. Palaeoecol.* **163**, 163–196 (2000).
43. Junium, C. K. & Arthur, M. A. Nitrogen cycling during the Cretaceous, Cenomanian-Turonian Oceanic Anoxic Event II. *Geochem. Geophys. Geosyst.* **8**, Q03002 (2007).
44. Thunell, R. C., Sigman, D. M., Muller-Karger, F., Astor, Y. & Varela, R. Nitrogen isotope dynamics of the Cariaco Basin, Venezuela. *Glob. Biogeochem. Cycles* **18**, GB3001 (2004).
45. Emmer, E. & Thunell, R. C. Nitrogen isotopic variation in Santa Barbara Basin sediments: Implications for denitrification in the Eastern Tropical North Pacific during the last 50,000 years. *Paleoceanography* **15**, 377–387 (2000).

Supplementary Information accompanies the paper at www.nature.com/naturegeoscience.

Acknowledgements

We thank W. Lynn Watney and the Kansas Geological Survey for access to the study cores, T. Phillips for drafting services and M. Altabet for a review of the manuscript. This project was supported by grants to T.J.A. from the National Science Foundation (EAR-0310072, EAR-0618003 and EAR-0745574) and the University of Cincinnati Research Council.

Author information

Reprints and permission information is available online at http://npg.nature.com/reprintsandpermissions. Correspondence and requests for materials should be addressed to T.A.